Atmos. Chem. Phys. Discuss., 9, 2763–2790, 2009
www.atmos-chem-phys-discuss.net/9/2763/2009/

Atmospheric Chemistry and Physics Discussions

This discussion paper is/has been under review for the journal *Atmospheric Chemistry and Physics (ACP)*. Please refer to the corresponding final paper in *ACP* if available.

Chinese SO_2 pollution over Europe – Part 2: Simulation of aerosol and cloud condensation nuclei formation

V. Fiedler[1,2], **F. Arnold**[2,1], **H. Schlager**[1], **and L. Pirjola**[3,4]

[1]Deutsches Zentrum für Luft- und Raumfahrt, Institut für Physik der Atmosphäre, Oberpfaffenhofen, 82234 Wessling, Germany
[2]Max Planck Institute for Nuclear Physics, (MPIK), Atmospheric Physics Division, P.O. Box 103980, 69029 Heidelberg, Germany
[3]Department of Physics, University of Helsinki, P.O. Box 64, 00014 Helsinki, Finland
[4]Department of Technology, Metropolia University of Applied Sciences, P.O. Box 4000, 00180 Helsinki, Finland

Received: 4 December 2008 – Accepted: 15 December 2008 – Published: 28 January 2009

Correspondence to: V. Fiedler (verena.fiedler@dlr.de)

Published by Copernicus Publications on behalf of the European Geosciences Union.

Abstract

We report on sulfur dioxide (SO_2) induced formation of aerosols and cloud condensation nuclei in an SO_2 rich aged (9 days) pollution plume of Chinese origin, which we have detected at 5–7 km altitude during a research aircraft mission over the East Atlantic off the West coast of Ireland. Building on our measurements of SO_2 and other trace gases along with plume trajectory simulations, we have performed model simulations of SO_2 induced formation of gaseous sulfuric acid (GSA, H_2SO_4) followed by GSA induced formation and growth of aerosol particles. We find that efficient photochemical SO_2 conversion to GSA took place in the plume followed by efficient formation and growth of H_2SO_4-H_2O aerosol particles. Most particles reached sufficiently large sizes to act as cloud condensation nuclei whenever water vapor supersaturation exceeded 0.1–0.2%. As a consequence, smaller but more numerous cloud droplets are formed, which tend to increase the cloud albedo and to decrease the rainout efficiency. The detected plume represents an interesting example of the environmental impact of long range transport of fossil fuel combustion generated SO_2.

1 Introduction

Fossil fuel combustion represents the most important source of atmospheric sulfur dioxide (SO_2), a major air pollutant. Presently most atmospheric SO_2 is released in Europe and China from combustion of relatively sulfur rich coal (Lelieveld et al., 2001). Sulfur dioxide impacts the environment in several ways. It is toxic and after inhalation may cause severe adverse health effects (e.g. Sunyer et al., 2003; Venners et al., 2003; Longo et al., 2008). Moreover, it contributes to atmospheric acidity and acid-induced corrosion (e.g. Rodhe et al., 2002; Huang et al., 2008). In the atmosphere, SO_2 undergoes conversion to particulate sulfate and OH-induced gas-phase conversion to gaseous sulfuric acid (GSA, H_2SO_4), (e.g. Menon and Saxena, 1998; Reiner and Arnold, 1993, 1994; Fiedler et al., 2005). At low temperatures typical of the middle

ACPD

9, 2763–2790, 2009

and upper troposphere, GSA may undergo binary (H_2SO_4-H_2O) nucleation leading to new aerosol particles. These grow by condensation and coagulation and ultimately may become CCN (Seinfeld and Pandis, 2006). Consequently, atmospheric SO_2 promotes the formation of sulfuric acid-water aerosol particles which impact the radiation balance by absorbing and scattering sunlight and by prolonging the lifetime of clouds (e.g. Ramanathan et al., 2001; Harshvardhan et al., 2002; Garrett et al., 2002; Andreae et al., 2005).

After SO_2 release from ground level combustion sources substantial amounts of SO_2 may be transported to the middle and upper troposphere and thereby escape deposition at the surface and are less affected by removal via cloud processes. In the middle and upper troposphere, SO_2 is removed preferably by OH induced gas-phase conversion to GSA which leads to a SO_2 lifetime of about 7–14 days depending on the efficiency of photochemical OH formation (e.g. Finlayson-Pitts and Pitts, 2000). Hence, the SO_2 lifetime is sufficiently long to allow SO_2 long-range transport. Therefore, SO_2 may impact aerosols and clouds thousands of kilometers away from its emission source. An interesting question is to what extent the important SO_2 source China impacts regional aerosols and clouds. Here we report on model investigations of SO_2 induced formation of GSA, aerosols and CCN in a major SO_2 rich pollution plume of Chinese origin, which we have detected over the East Atlantic (Fiedler et al., 2008). The model simulations are performed with an atmospheric chemistry and aerosol dynamics model AEROFOR (Pirjola, 1999; Pirjola and Kulmala, 2001).

Previous comparable AEROFOR model examples have been published e.g. by Pirjola et al. (1999) and by Laaksonen et al. (2000).

This paper consists of the following sections: Sect. 2 presents a short review of the SO_2 measurements off the Irish west coast. Section 3 describes the AEROFOR model simulation inputs, the model results and discusses the sensitivity of the results to several input parameters. Section 4 interprets the model simulations further concerning the SO_2 impact on CCN formation.

ACPD
9, 2763–2790, 2009

2 Measurements

The measurements are described in detail in the accompanying paper "Chinese SO_2 pollution over Europe – Part 1" (Fiedler et al., 2008). The measurement flight started from Brest in Northern France on 3 May 2006 and took place over the Atlantic Ocean south and west of Ireland. The SO_2 measurement method was chemical ionization mass spectrometry (CIMS) using a permanent calibration with isotopically labeled SO_2. The objective was to probe an Asian pollution plume, which had been predicted before by the lagrangian particle dispersion model FLEXPART (Stohl et al., 2002, 2005). Between 10:00 and 11:00 UTC several pollution plumes were detected as particularly indicated by very markedly elevated SO_2. A comprehensive description of the measurements especially in the light of other simultaneously measured trace gases can be found in Fiedler et al. (2008).

Figure 1 shows the vertical distribution of the SO_2 mole fraction measured during that flight. Apart from a SO_2 pollution layer of American origin at approximately 1.5 km altitude, a deep layer of SO_2 has been detected in the altitude range from 5 to 7.5 km. The atmospheric SO_2 background in this layer is about 150 pmol/mol with a single peak of 900 pmol/mol which is discussed in detail in the accompanying paper Fiedler et al. (2008).

FLEXPART particle dispersion model analyses identified a region in North East China as the source region of the SO_2 emissions.

3 Aerosol model simulations

3.1 Initialization of the model

The air mass with the highest SO_2 mole fraction (around 10:40 UTC, e.g. in Fig. 3 of the paper Fiedler et al., 2008) was investigated using simulations by the atmospheric chemistry and aerosol dynamics model AEROFOR along the trajectory. This model

ACPD
9, 2763–2790, 2009

has previously been described (e.g. Pirjola, 1999; Pirjola and Kulmala, 2001). AEROFOR is a sectional box model which treats aerosol formation by homogeneous binary nucleation of H_2SO_4 and H_2O (Vehkamäki et al., 2002) as well as aerosol growth by H_2SO_4-H_2O condensation (Fuchs and Sutugin, 1971) and aerosol coagulation (Fuchs, 1964). In this work a Lagrangian approach is used. From a prescribed SO_2 and OH concentration the H_2SO_4 concentration is calculated. Further model input needed is an initial particle concentration, pressure, relative humidity and temperature along the trajectory. The model then delivers the homogeneous binary nucleation rate J_{honu}, condensation sink CS, which is principally the inverse H_2SO_4 lifetime, and particle number size distributions between 0.86 nm and 1 μm. In this work we used 54 size bins.

The particle concentration calculation in the model moreover builds on a bimodal initial particle size distribution, possessing the lognormal parameters

$$N_1 = 200\ cm^{-3} \quad (1)$$

$$d_1 = 130\ nm \quad (2)$$

$$\sigma_1 = 1.45 \quad (3)$$

and

$$N_2 = 50\ cm^{-3} \quad (4)$$

$$d_2 = 250\ nm \quad (5)$$

$$\sigma_2 = 1.9 \quad (6)$$

with N_1 the initial particle number concentration in mode 1, d_1 the geometric mean diameter of that mode and σ_1 the geometric standard deviation of the lognormal distribution, N_2, d_2 and σ_2 respectively in mode 2. Here, four different scenarios (A, B, C, D) will be investigated for the highest SO_2 peak. Since no measurements existed for the preexisting particle size distribution, the initial particle concentrations are varied by multiplying the above values by 0, 1, 2 and 4, resulting in total initial particle concentrations of 0, 250, 500 and 1000 cm^{-3}.

ACPD
9, 2763–2790, 2009

The simulation time is 8.5 days starting at 00:00 UTC on 25th of April 2006, so ending around noon on the 3rd of May 2006, which was the measurement flight day and time. The initial SO_2 concentration of 4.4×10^{10} cm^{-3} was chosen in such a way that the final modeled SO_2 concentration (1.3×10^{10} cm^{-3}, which corresponds at that temperature and pressure level to 900 pmol/mol) matches the measured SO_2. At the beginning of the simulation the air parcel under consideration was lifted to 8 km (≈335 hPa). Table 1 summarizes the model input data of the four model cases.

For the OH calculation a clear sky assumption was made. This is in accordance with a rough satellite cloud top temperature data analysis. Latitude, longitude and time in UTC have been taken into account as well as the length of the day. Typical maximum OH concentrations were adopted from Logan et al. (1981). In Fig. 2 6 h mean values of temperature and relative humidity, RH, calculated from the water vapor concentration along the trajectory are plotted. The temperature stays rather constant around 240 K the whole time, relative humidity varies between 5% and 68% with two maxima at the beginning and on day 6 of the simulation. We also calculated the saturation vapor pressure over ice based on the Magnus equation (Pruppacher and Klett, 2000) and the relative humidity over ice, RHice, also shown in Fig. 2. Since for temperatures below 0°C the water vapor saturation pressure over liquid water is always higher than over ice, RHice is higher than RH for the same atmospheric water vapor concentration. However, water vapor supersaturation does not occur in the 8.5 simulation days.

3.2 Model results

Figures 3–8 describe the AEROFOR model results. All times are in UTC. Figures 3 and 4 show the model results for model scenario A with an initial particle concentration of 0 cm^{-3}. Plotted versus time are: SO_2 concentration, GSA and prescribed OH, rate J of H_2SO_4-H_2O nucleation, and number concentrations Nd of aerosol particles with diameters larger than d nm. The OH (Fig. 3, upper panel) undergoes a semi-sinusoidal diurnal variation with maximum local noontime OH concentrations of about $2–4\times10^6$ cm^{-3} depending mostly on geographic latitude. The OH converts SO_2 to GSA and causes,

ACPD
9, 2763–2790, 2009

within the 8.5 days of simulation, SO_2 to decrease from 4.4×10^{10} cm^{-3} (corresponding to a mole fraction of almost 3700 pmol/mol) to 1.3×10^{10} cm^{-3} (corresponding to the measured maximum mole fraction of around 900 pmol/mol). In comparison, the FLEXPART particle dispersion model predicted a SO_2 mole fraction of 2500–3500 pmol/mol at the location and time of our measurement (paper 1, Fig. 9, Fiedler et al., 2008). Considering that FLEXPART treats SO_2 as an inert tracer, this compares well to the assumption of 3700 pmol/mol as initial SO_2 mole fraction input for the AEROFOR model.

After 8.5 days, about 70% of the initially available SO_2 has undergone photochemical conversion to GSA, which in turn has been incorporated into aerosol particles. The H_2SO_4 concentration (Fig. 3, upper panel) shows a diurnal variation, following the diurnal variation of OH. Right in the beginning, H_2SO_4 local noontime concentrations of 3×10^7 cm^{-3} are reached. The maximum varies slightly each day between 1×10^7 and 3×10^7 cm^{-3}. The homogeneous nucleation rate J_{honu} (Fig. 3, lower panel) shows two strong maxima around noon on day 0 and day 1 (7000 and 20 000 cm^{-3} s^{-1}) and three smaller peaks on day 2 and 6, which corresponds to the local minima in temperature accompanied by local maxima in relative humidity. Low temperatures and high relative humidities favor new particle formation. The condensation sink CS (Fig. 4, lower panel) starts at 0 s^{-1} as no initial particles exist, but increases immediately to 0.01 s^{-1} simultaneously to the occurring nucleation. During nighttime the CS decreases caused by the decrease in the total particle surface, which results from coagulation and growth of the existing particles. The surface to volume ratio decreases with increasing radius of the particles. So, if small particles coagulate to form bigger ones, the total aerosol surface will decrease. This means that the total aerosol surface available for gaseous sulfuric acid scavenging decreases during night, if no new particles are formed. After the new nucleation on simulation day 1 the CS reaches its maximum of 0.013 s^{-1}. Eventually, this results in the particle concentrations depicted in Fig. 4, upper panel. A strong increase in the total particle concentration (up to 6×10^6 cm^{-3}), caused by the two nucleation bursts on the first and second day of the simulation, is followed by a slow decrease of the total particles to a final value of ≈1600 cm^{-3}. Condensational

ACPD
9, 2763–2790, 2009

and coagulational growth of the freshly formed particles forms particles with diameters larger than 30 nm already on the first day. Particles of these size classes may act as cloud condensation nuclei (CCN) and are therefore available for cloud formation.

Similar graphs for model scenario B with an initial particle concentration of 250 cm^{-3} are not shown as no major changes occurred compared to scenario A. In model case B, H_2SO_4 concentration and homogeneous nucleation rate show nearly the same behavior as in model case A. The CS starts at 0.002 s^{-1} instead of 0 s^{-1}, because of the initial particles that are available for condensation already when the simulation starts. However, the CS maximum value is 0.013 s^{-1} as in scenario A. Freshly nucleated particles are formed in the same amount as in scenario A, so there is obviously enough H_2SO_4 available for both, growth of the initial particles and nucleation of new ones. The formation of CCN after 1 day is still enhanced and a final total particle concentration of 1300 cm^{-3} at the measurement site can be expected.

The plots for model scenario C (initial particle concentration 500 cm^{-3}) are shown in Figs. 5 and 6. The higher initial particle concentration again has no substantial influence on the H_2SO_4 concentration and the nucleation rate, but the higher CS (starting at 0.005 s^{-1} and 0.0135 s^{-1} in maximum) slows down the growth of the particles particularly in the size classes N50, N100 and N200. The growth starts one day later than in scenario A and the total increase in the number concentration of CCN is less developed. Nevertheless the final concentration of CCN reaches in the sum of initial and freshly formed particles 1200 cm^{-3}.

Model scenario D, depicted in Figs. 7 and 8, eventually starts with the assumption of 1000 cm^{-3} as initial particle concentration, which is almost the final value in scenario C. The H_2SO_4 concentration development stays nearly the same, but the nucleation rate J_{honu} is slightly lowered. The condensation sink is further increasing and is all the time above 0.01 s^{-1} with a maximum of 0.0143 s^{-1}. The increase in the total particle concentration on the first two simulation days is still appreciable, but the growth in all size classes is now markedly reduced. So the H_2SO_4 concentration seems still to be high enough for new particle formation, but a large amount of H_2SO_4 will be

ACPD
9, 2763–2790, 2009

already consumed by condensation onto preexisting particles, so that not much H_2SO_4 is left for condensation on newly formed particles. The final concentration of CCN is approximately 700 cm^{-3}.

Typical previously measured particle concentrations for background aerosol are around 500 cm^{-3} and in very polluted cases also several 1000 cm^{-3} can be reached (e.g., Minikin et al., 2003). So at least model scenario C seems to be quite realistic.

With even higher initial particle concentrations (e.g. 2000 cm^{-3}) nucleation would not occur at all due to a complete removal of the condensable gases by condensation onto the preexisting aerosol.

Figure 9 gives an overview of the modeled final particle concentrations N30, N100 and N200 (after 8.5 days). For comparison, the corresponding initial particle concentrations are also given. The right panel of Fig. 9 shows model predictions with H_2SO_4 formation switched off. Here new aerosol formation does not occur and preexisting particles grow only by coagulation. For increasing preexisting particle concentrations coagulation becomes more efficient resulting in a decrease of N30 and N100 with respect to the corresponding concentrations at time 0. In contrast, N200 increases but the increase is only very small. When photochemical SO_2 conversion to H_2SO_4 is switched on, the situation changes drastically (Fig. 9, left panel). Now, for each of the 4 scenarios A, B, C and D, the final concentrations of N30, N100 and N200 are much larger. Hence, the AEROFOR model simulations indicate very substantial SO_2-mediated growth of preexisting and newly formed aerosol particles.

3.3 Sensitivity analyses

The simulation of the model case C was repeated to test the sensitivity of the concentration of CCN after 8.5 days against the initial SO_2 concentration, OH concentration, nucleation rate and initial particle size distribution.

When multiplying the nucleation rate by a factor of 100 and keeping the OH and SO_2 concentrations as in case C the final N50, N100 and N200 increased only 4%, 7% and 2%, respectively. The total particle concentration became threefold but the major part

of the particles remained smaller than 4 nm in diameter size. Thus we can conclude that the CCN production is much more sensitive to particle growth, i.e. condensable vapor concentration, than to the actual nucleation rate.

Since the GSA formation rate is proportional to $OH \times SO_2$, the simulations were repeated by multiplying first the OH by a factor of 2 (SO_2 as in case C) and then the initial SO_2 by a factor of 2 (OH as in case C). The final SO_2 concentration was 4.5×10^9 cm^{-3} (≈305 pmol/mol) and 2.8×10^{10} cm^{-3} (≈1900 pmol/mol), respectively. The increases in N50, N100 and N200 were 16%, 41% and 35%, and 25%, 67% and 92%, respectively.

The other factor which affects the growth of nucleated particles is the condensation sink CS of the preexisting particles. The CS is mainly determined by the number concentration and the size distribution of the preexistent particles. Therefore, a CS sensitivity study is already included in the 4 simulation cases. The CS of case B (initial particle concentration of 250 cm^{-3}) e.g. corresponds to the CS of case C (initial particle concentration of 500 cm^{-3}) if the diameter of the particles in mode 1 of case C (N1=400 cm^{-3}) is changed to 62 nm and the diameter in mode 2 of case C (N2=100 cm^{-3}) is changed to 124 nm (see also Table 1 for comparison). On the other hand, if the diameters of the particles in mode 1 and 2 of case D are changed to 100 nm and 200 nm, respectively, the CS of case B is the same CS as in case D.

4 Implications for CCN

Our above findings have interesting implications for CCN and cloud droplet formation. In the atmosphere, water vapor supersaturation (WSS) occasionally occurs and aerosol particles with sufficiently large diameters and hygroscopicity may act as CCN and induce water cloud droplet formation. Mostly, WSS is induced by adiabatic cooling or mixing of air masses with different temperatures and humidities (e.g. Seinfeld and Pandis, 2006; Gettelman et al., 2006). Typical atmospheric water vapor supersaturation rarely surpasses 2%, the median of observed supersaturation even is 0.1% (Pruppacher and Klett, 2000).

ACPD
9, 2763–2790, 2009

Sulfuric acid is very hygroscopic and therefore H_2SO_4 represents an ideal CCN material. H_2SO_4-H_2O aerosols are liquid in the temperature and RH conditions encountered in the troposphere. While H_2SO_4 contained in an aerosol droplet may promote water vapor uptake, it may at least initially hinder droplet freezing depending on the H_2SO_4 fraction of the droplet mass (Carleton et al., 1997; Ettner et al., 2004). As water vapor uptake proceeds and the droplet size has increased sufficiently and the H_2SO_4 mass fraction has decreased sufficiently, the droplet may ultimately freeze even quasi-homogeneously, depending on RHi. However, a pure water droplet only freezes at Temperatures <235 K and RHi>145%. Those values have not been reached during the 8.5 simulation days (Fig. 2). Figure 10 depicts the minimum diameter a H_2SO_4-H_2O aerosol particle needs to possess in order to become a water vapor condensation nucleus (activation diameter). For example for WSS=0.5%, the critical diameter is about 56 nm. As suggested by our above AEROFOR model simulations, in the Chinese pollution plume even newly formed particles grow to diameters larger than 50 nm within only a few days and therefore will act as CCN at WSS=0.5%. For lower WSS the minimum diameter increases very steeply (Fig. 10), which is due to the Kelvin effect.

Figure 11 shows the modeled number concentration of CCN sized H_2SO_4-H_2O aerosol particles versus WSS. CCN concentrations refer to the end of the simulation period and to the four model cases A (Nini=0), B (Nini=250) etc. The right panel is the model with gaseous sulfuric acid formation switched off. Here particles grow only due to coagulation. In this case for models B, C and D the CCN concentrations increase initially steeply with WSS which means that an increasing fraction of the particles can act as CCN. For WSS>0.4% (critical diameter: 65 nm), CCN concentrations remain nearly constant, which means that all particles present at the end of the simulation period act as CCN. Due to coagulation, during the simulation period, their total number concentration has decreased and their diameters have increased. The left panel of Fig. 11 shows the model results with gaseous sulfuric acid formation switched on. Now, H_2SO_4-H_2O nucleation generates new particles and both, new and preexisting particles grow by H_2SO_4-H_2O condensation and coagulation. Now, for WSS>0.1% (critical

diameter=163 nm), CCN concentrations become mostly (with exception of model case D) much larger than for the model without GSA formation since numerous newly formed particles become CCN. For WSS<0.1%, CCN concentrations are largest for case D and smallest for case A, which is similar to the case without GSA formation (bottom panel). For WSS>0.1%, CCN concentrations are largest for case A and smallest for case D. For WSS>0.5%, CCN concentrations become nearly constant. This means that all particles, including even the newly formed ones, become CCN.

Our findings suggest that, already on day 6, the Chinese pollution plume had developed its full CCN potential (maximum N100) and was primed for the formation of large concentrations of relatively small water droplets whenever WSS of about 0.2% built up (activation diameter 100 nm for 0.2% WSS, view Fig. 10). Condensation of a given mass of supersaturated water vapor on more CCN leads to smaller and more numerous cloud droplets. This tends to increase the albedo of the cloud and to increase the cloud lifetime with respect to rainout, since the droplet sedimentation velocity is approximately proportional to the square of the droplet diameter. In other words, after 9 days and at a distance of about 20 000 km from its birthplace, the plume had very suitable conditions for the formation of whiter clouds possibly possessing a reduced tendency for rainout. The Chinese pollution plume reported here represents a striking example of an environmental impact of long range transport of fossil fuel combustion generated SO_2.

5 Conclusions

We have investigated aerosol and CCN formation in a SO_2 rich pollution plume of Chinese origin which had traveled within 9 days from China to Europe where we have detected the plume at 5–7 km altitude during an aircraft mission by measuring SO_2. During most of the plume travel clouds were absent inside and above the plume and therefore efficient photochemical conversion of SO_2 to GSA took place, followed by GSA induced formation and growth of H_2SO_4-H_2O aerosol particles. Our AEROFOR

ACPD
9, 2763–2790, 2009

model simulations of aerosol and CCN formation lead to the following conclusions: in the plume, high SO_2 induced a strong increase of the concentration of H_2SO_4-H_2O aerosol particles sufficiently large to act as cloud condensation nuclei already at a water vapor supersaturation exceeding only 0.1%. This implies that whenever WSS exceeded 0.1–0.2% in the 9 days aged plume, smaller and more numerous cloud droplets were formed. This tends to increase the cloud albedo and to decrease the tendency for rainout. The investigated Chinese pollution plume represents an interesting example of a potential environmental impact of long range transport of fossil fuel combustion generated SO_2.

Acknowledgements. The authors gratefully acknowledge A. Dörnbrack (DLR) for providing ECMWF temperature and humidity data along the backward trajectories as model input data. The DWD is acknowledged to provide access to the ECMWF analysis data. We are grateful to the crew of the DLR Flight Department for their commitment and support to collect this data set. We also thank Bernd Kärcher (DLR) for the fruitful discussions and comments. This work was funded by DLR, MPI-K and Metropolia University of Applied Sciences, Helsinki. The data analysis was also supported in part by the Deutsche Forschungsgemeinschaft (DFG) within the Priority Program HALO under contract SPP1294.

This Open Access Publication is financed by the Max Planck Society.

References

Andreae, M., Jones, C., and Cox, P.: Strong present-day aerosol cooling implies a hot future, Nature, 435, 1187–1190, 2005. 2765

Carleton, K., Sonnenfroh, D., , Rawlins, W., Wyslouzil, B., and Arnold, S.: Freezing behavior of single sulfuric acid aerosols suspended in a quadrupole trap, J. Geophys. Res., 102, 6025–6033, 1997. 2773

Ettner, M., Mitra, S., and Borrmann, S.: Heterogeneous freezing of single sulfuric acid solution droplets: laboratory experiments utilizing an acoustic levitator, Atmos. Chem. Phys., 4, 1925–1932, 2004, http://www.atmos-chem-phys.net/4/1925/2004/. 2773

Fiedler, V., Dal Maso, M., Boy, M., Aufmhoff, H., Hoffmann, J., Schuck, T., Birmili, W., Hanke, M., Uecker, J., Arnold, F., and Kulmala, M.: The contribution of sulphuric acid to atmospheric particle formation and growth: a comparison between boundary layers in Northern and Central Europe, Atmos. Chem. Phys., 5, 1773–1785, 2005, http://www.atmos-chem-phys.net/5/1773/2005/. 2764

Fiedler, V., Nau, R., Ludmann, S., Arnold, F., Schlager, H., and Stohl, A.: Chinese SO_2 pollution over Europe – Part 1: Airborne trace gas measurements and source identification by particle dispersion model simulations, Atmos. Chem. Phys. Discuss., 9, 1377–1405, 2009, http://www.atmos-chem-phys-discuss.net/9/1377/2009/. 2765, 2766, 2769

Finlayson-Pitts, B. J. and Pitts, J. N. J.: Chemistry of the upper and lower atmosphere, Academic Press, San Diego, London, first edn., 2000. 2765

Fuchs, N.: The Mechanics of Aerosols, Pergamon Press, London, 1964. 2767

Fuchs, N. and Sutugin, A.: Highly dispersed aerosol, in: Topics in current aerosol research, edited by: Hidy, G. M. and Brock, J. R., Pergamon, New York, 1971. 2767

Garrett, T., Radke, L., and Hobbs, P.: Aerosol Effects on Cloud Emissivity and Surface Longwave Heating in the Arctic, J. Atmos. Sci., 59, 769–778, 2002. 2765

Gettelman, A., Fetzer, E., Eldering, A., and Irion, F.: The Global Distribution of Supersaturation in the Upper Troposphere from the Atmospheric Infrared Sounder, J. Climate, 19, 6089–6103, 2006. 2772

Harshvardhan, Schwarz, S., Benkovitz, C., and Guo, G.: Aerosol Influence on Cloud Microphysics Examined by Satellite Measurements and Chemical Transport Modelling, J. Atmos. Sci., 59, 714–725, 2002. 2765

Huang, K., Zhuang, G., Xu, C., Wang, Y., and Tang, A.: The chemistry of the severe acidic precipitation in Shanghai, China, Atmos. Res., 89, 149–160, 2008. 2764

Laaksonen, A., Pirjola, L., Kulmala, M., Arnold, F., Raes, F., and Wohlfrom, K.-H.: Upper tropospheric SO_2 conversion into sulfuric acid aerosols and cloud condensation nuclei, J. Geophys. Res., 105, 1459–1469, 2000. 2765

Lelieveld, J., Crutzen, P. J., and Ramanathan, V., et al.: The Indian Ocean Experiment: Widespread Air Pollution from South and Southeast Asia, Science, 291, 1031, doi:

10.1126/science.1057103, 2001. 2764
Logan, J., Prather, M., Wofsy, S., and McElroy, M.: Tropospheric Chemistry: A Global Perspective, J. Geophys. Res., 86, 7210–7254, 1981. 2768
Longo, B., Rossignol, A., and Green, J.: Cardiorespiratory health effects associated with sulphurous volcanic air pollution, Public Health, 122, 809–820, 2008. 2764
Menon, S. and Saxena, V.: Role of sulfates in regional cloud-climate interactions, Atmos. Res., 47–48, 299–315, 1998. 2764
Minikin, A., Petzold, A., Ström, J., Krejci, R., Seifert, M., van Velthoven, P., Schlager, H., and Schumann, U.: Aircraft observations of the upper tropospheric fine particle aerosol in the Northern and Southern Hemispheres at midlatitudes, Gophys. Res. Lett., 30, 1503, 2003. 2771
Pirjola, L.: Effects of the increased UV radiation and biogenic VOC emissions on ultrafine aerosol formation, J. Aerosol Sci., 30, 355–367, 1999. 2765, 2767
Pirjola, L. and Kulmala, M.: Development of particle size and composition distribution with a novel aerosol dynamics model, Tellus, 53B, 491–509, 2001. 2765, 2767
Pirjola, L., Kulmala, M., Wilck, M., Bischoff, A., Stratmann, F., and Otto, E.: Formation of sulphuric acid aerosols and cloud condensation nuclei: An expression for significant nucleation and model comparison, J. Aerosol Sci., 30, 1079–1094, 1999. 2765
Pruppacher, H. and Klett, J.: Microphysics of clouds and precipitation, Kluwer Academic Publishers, Dordrecht, The Netherlands, 2000. 2768, 2772
Ramanathan, V., Crutzen, P., Kiehl, J., and Rosenfeld, D.: Aerosol, climate, and the hydrological cycle, Science, 294, 2119–2124, 2001. 2765
Reiner, T. and Arnold, F.: Laboratory flow reactor measurements of the reaction SO_3+H_2O + M→ H_2SO_4+M: Implications for gaseous H_2SO_4 and aerosol formation in the plume of jet aircraft, Geophys. Res. Lett., 20, 2659–2662, 1993. 2764
Reiner, T. and Arnold, F.: Laboratory investigations of gaseous sulfuric acid formation via SO_3 + H_2O + M → H_2SO_4 + M: Measurements of the rate constant and products identification, J. Chem. Phys., 101, 7399–7407, 1994. 2764
Rodhe, H., Dentener, F., and Schulz, M.: The Global Distribution of Acidifying Wet Deposition, Environ. Sci. Technol., 36, 4382–4388, 2002. 2764
Seinfeld, J. and Pandis, S.: Atmospheric Chemistry and Physics, John Wiley & Sons, Inc., second edn., 2006. 2765, 2772
Stohl, A., Eckhardt, S., Forster, C., James, P., Spichtinger, N., and Seibert, P.: A replacement

for simple back trajectory calculations in the interpretation of atmospheric trace substance measurements, Atmos. Environ., 36, 4635–4648, 2002. 2766

Stohl, A., Forster, C., Frank, A., Seibert, P., and Wotawa, G.: Technical note: The Lagrangian particle dispersion model FLEXPART version 6.2, Atmos. Chem. Phys., 5, 2461–2474, 2005, http://www.atmos-chem-phys.net/5/2461/2005/. 2766

Sunyer, J., Atkinson, R., Ballester, F., Le Tertre, A., Ayres, J., Forastiere, F., Forsberg, B., Vonk, J., Bisanti, L., Anderson, R., Schwartz, J., and Katsouyanni, K.: Respiratory effects of sulphur dioxide: a hierarchical multicity analysis in the APHEA 2 study, Occu. Environ. Med., 60, doi:10.1136/oem.60.8.e2, 2003. 2764

Vehkamäki, H., Kulmala, M., Napari, I., Lehtinen, K., Timmreck, C., Noppel, M., and Laaksonen, A.: An improved parameterization for sulfuric acid-water nucleation rates for tropospheric and stratospheric conditions, J. Geophys. Res., 107, 4622, doi:10.1029/2002JD002184, 2002. 2767

Venners, S., Wang, B., Xu, Z., Schlatter, Y., Wang, L., and Xu, X.: Particulate matter, sulfur dioxide, and daily mortality in Chongqing, China., Environ. Health Perspect., 111, 562–567, 2003. 2764

Table 1. Number concentration of initial particles N_1 (130 nm diameter) and N_2 (250 nm diameter) in the four model cases A–D. The initial SO_2 concentration was in all cases the same.

Model Case	A	B	C	D
Initial Particles N_1 [cm^{-3}]	0	200	400	800
Initial Particles N_2 [cm^{-3}]	0	50	100	200
Initial SO_2 concentration [cm^{-3}]	4.4×10^{10}			

ACPD
9, 2763–2790, 2009

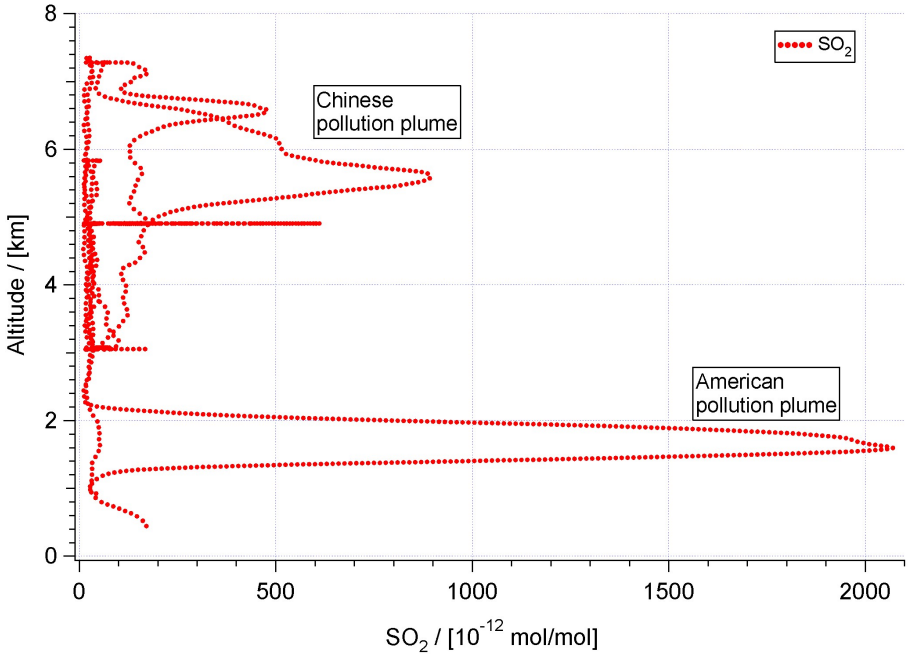

Fig. 1. SO_2 mole fraction altitude profile of flight 20060503, smoothed with a running mean averaging 30 data points.

ACPD
9, 2763–2790, 2009

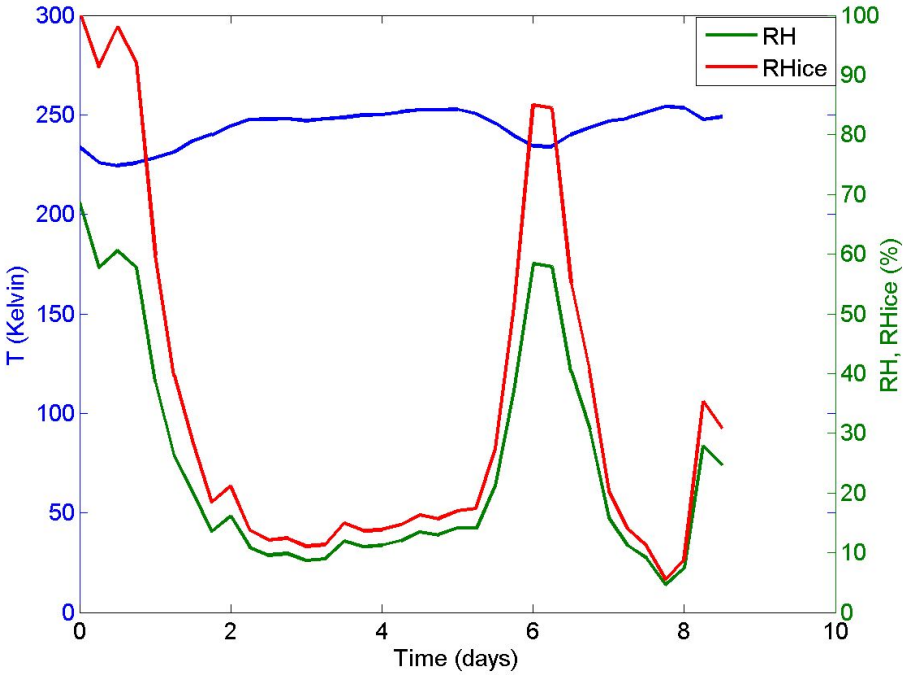

Fig. 2. AEROFOR model simulation input: temperature (blue) and relative humidity over water (green) and over ice (red) along the air mass back trajectory.

ACPD
9, 2763–2790, 2009

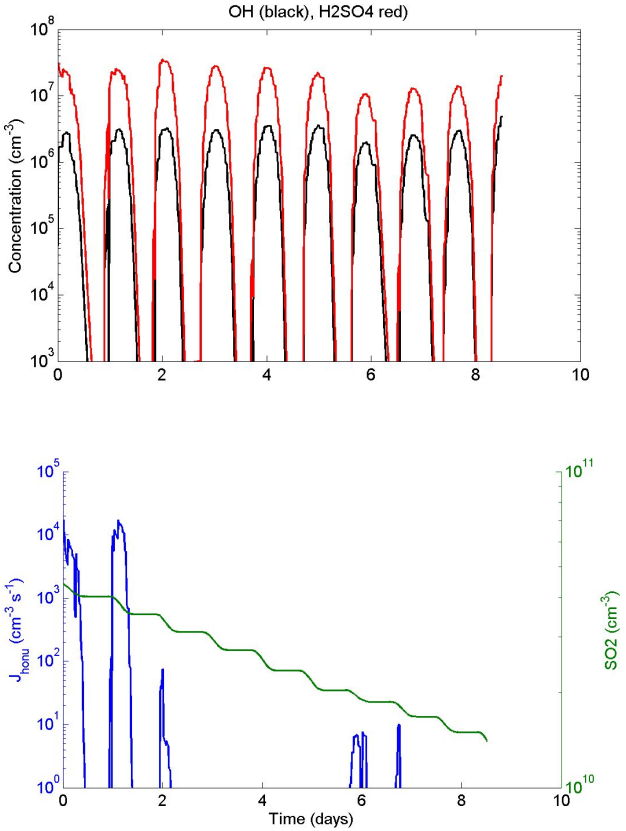

Fig. 3. AEROFOR simulation scenario A: no initial particle concentration. Upper panel: modeled OH and H_2SO_4 concentrations. Lower panel: homogeneous nucleation rate J_{honu} and SO_2 concentration.

ACPD
9, 2763–2790, 2009

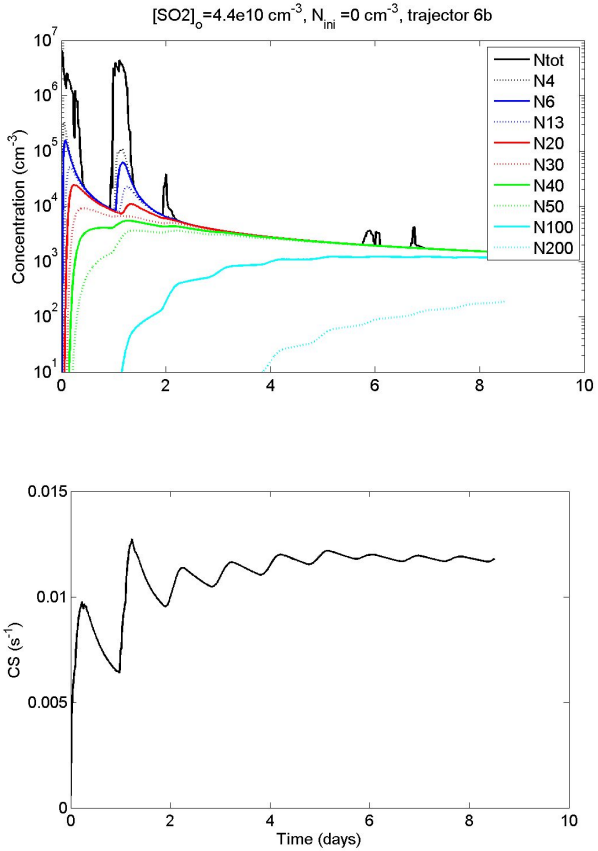

Fig. 4. AEROFOR simulation scenario A: no initial particle concentration. Upper panel: particle concentrations of particles of different size classes. Lower panel: condensation sink CS.

ACPD
9, 2763–2790, 2009

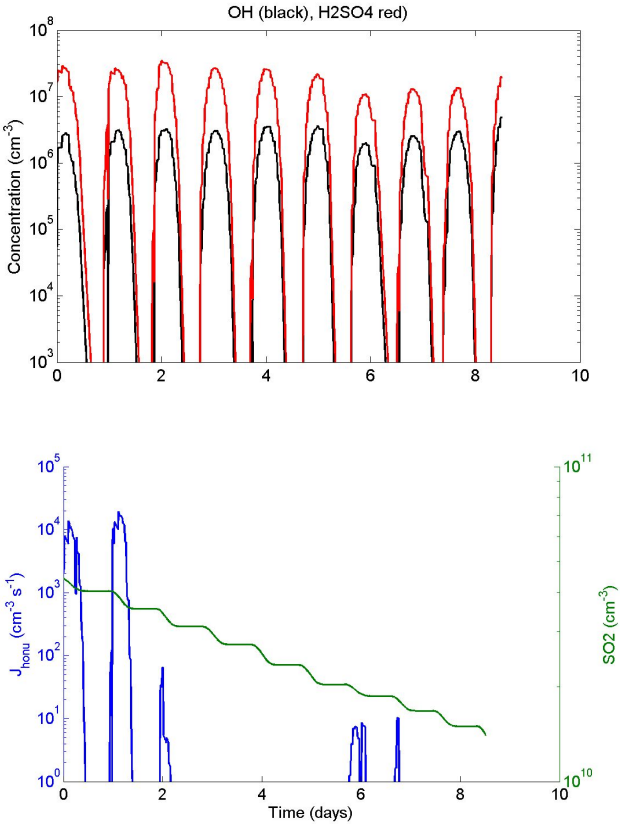

Fig. 5. AEROFOR simulation scenario C: initial particle concentration 500 cm^{-3}. Upper panel: modeled OH and H_2SO_4 concentrations. Lower panel: homogeneous nucleation rate J_{honu} and SO_2 concentration.

ACPD
9, 2763–2790, 2009

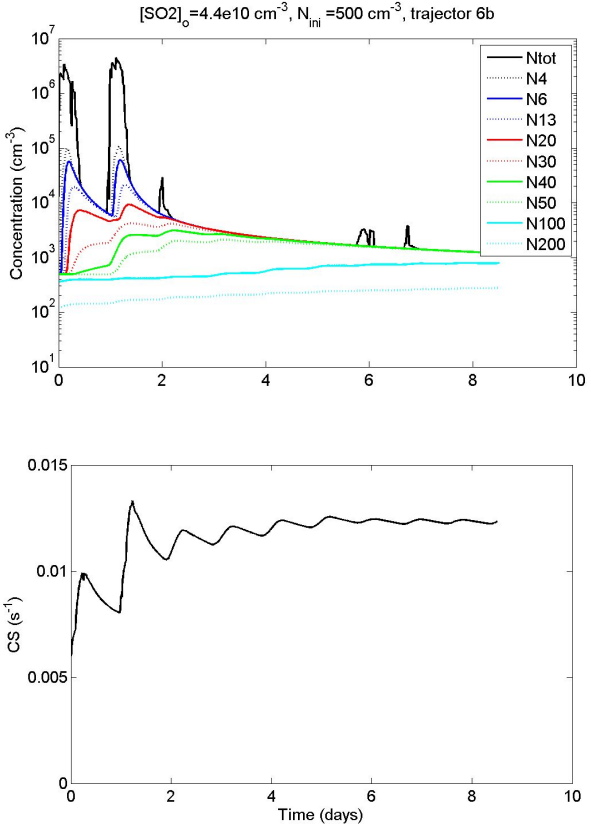

Fig. 6. AEROFOR simulation scenario C: initial particle concentration 500 cm^{-3}. Upper panel: particle concentrations of particles of different size classes. Lower panel: condensation sink CS.

ACPD
9, 2763–2790, 2009

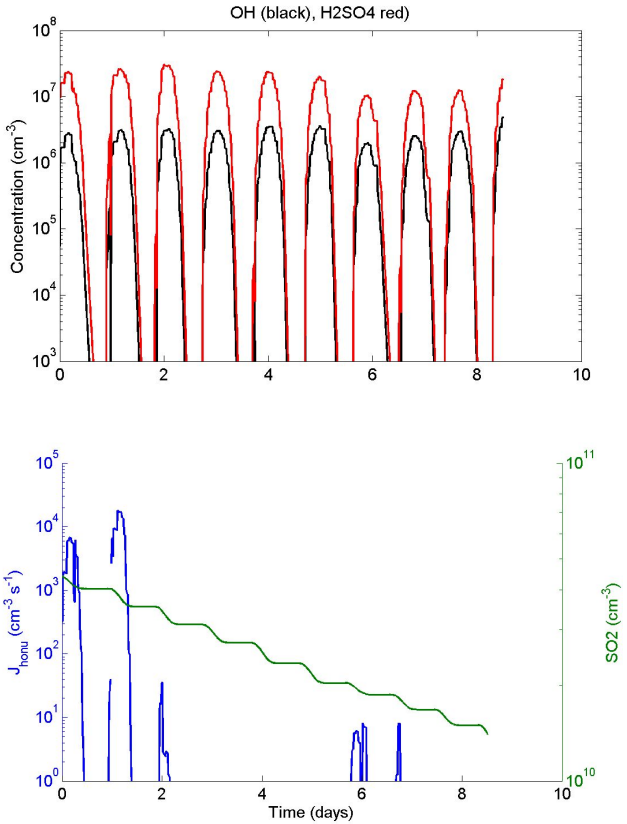

Fig. 7. AEROFOR simulation scenario D: initial particle concentration 1000 cm^{-3}. Upper panel: modeled OH and H_2SO_4 concentrations. Lower panel: homogeneous nucleation rate J_{honu} and SO_2 concentration.

ACPD
9, 2763–2790, 2009

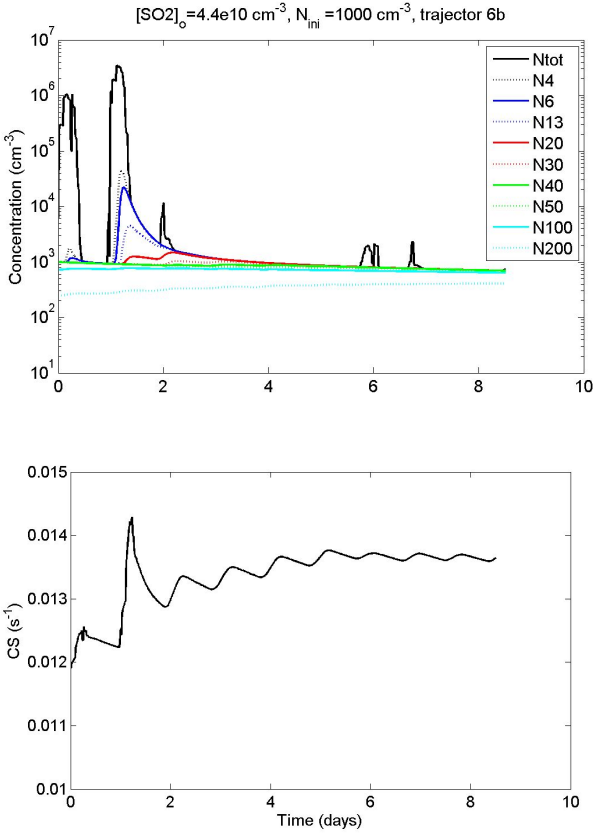

Fig. 8. AEROFOR simulation scenario D: initial particle concentration 1000 cm^{-3}. Upper panel: particle concentrations of particles of different size classes. Lower panel: condensation sink CS.

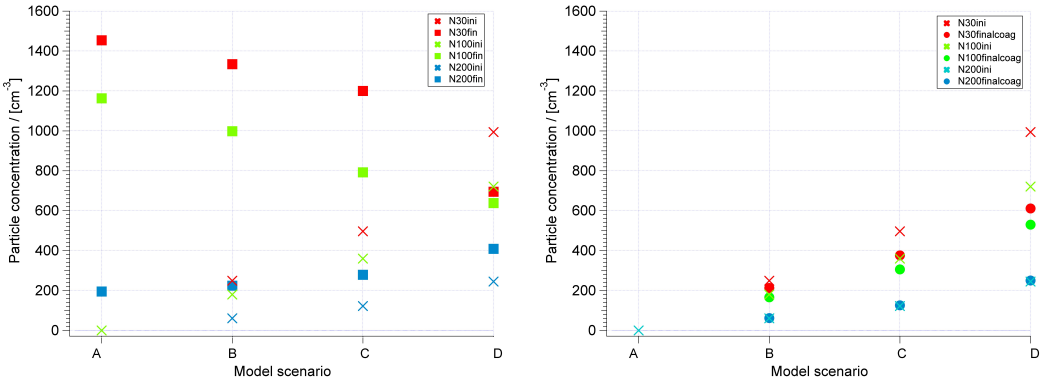

Fig. 9. Right panel: Particle concentrations for the four different model simulation cases initially (crosses) and after 8.5 simulation days (dots) if only coagulation is considered. Left panel: Particle concentrations initially (crosses) and after 8.5 simulation days (squares) if photochemical SO_2 conversion to H_2SO_4 is switched on.

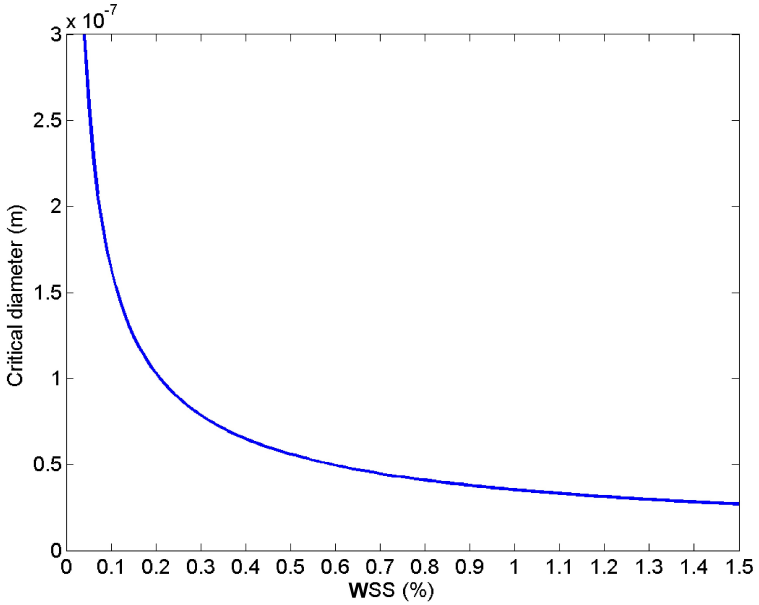

Fig. 10. The critical activation diameter of a H_2SO_4-H_2O CCN as a function of water vapor supersaturation WSS.

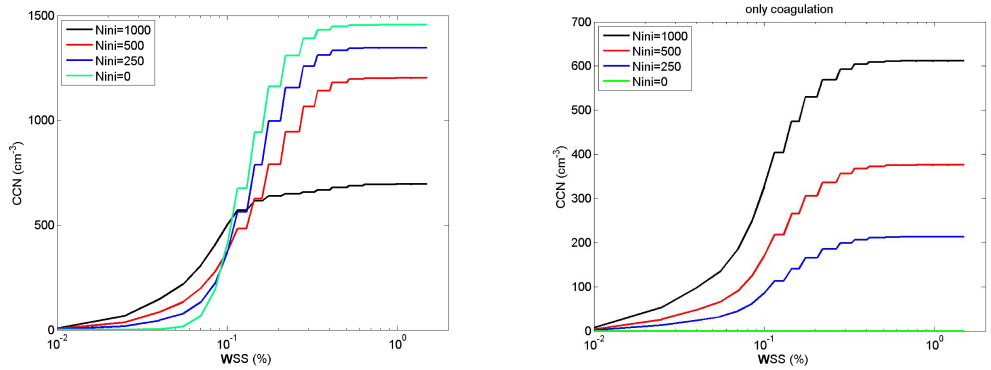

Fig. 11. Modeled number concentration of CCN sized H_2SO_4-H_2O aerosol particles versus water vapor supersaturation WSS. CCN concentrations refer to the end of the simulation period. The four model cases (Nini=0, 250, 500, 1000 cm^{-3}) are considered. Right panel is the model with gaseous sulfuric acid formation switched off. Mind the different y-axis scaling.

ACPD
9, 2763–2790, 2009